

Inhomogeneous phases in a double-exchange magnet with long range Coulomb interactions

Gideon Wachtel and Dror Orgad

Racah Institute of Physics, The Hebrew University, Jerusalem 91904, Israel

Denis I. Golosov

Department of Physics and the Resnick Institute, Bar-Ilan University, Ramat-Gan 52900, Israel

(Received 17 August 2008; revised manuscript received 16 October 2008; published 24 November 2008)

We consider a model with competing double-exchange (ferromagnetic) and superexchange (antiferromagnetic) interactions in the regime where phase separation takes place. The presence of a long range Coulomb interaction frustrates a macroscopic phase separation and favors microscopically inhomogeneous configurations. We use the variational Hartree-Fock approach, in conjunction with Monte Carlo simulations, to study the geometry of such configurations in a two-dimensional system. We find that an array of diamond-shaped ferromagnetic droplets is the preferred configuration at low electronic densities, while alternating ferromagnetic and antiferromagnetic diagonal stripes emerge at higher densities. These findings are expected to be relevant for thin films of colossal magnetoresistive manganates.

DOI: [10.1103/PhysRevB.78.184433](https://doi.org/10.1103/PhysRevB.78.184433)

PACS number(s): 75.47.Gk, 75.30.Kz, 75.10.Lp

I. INTRODUCTION

In recent years, doped manganese oxides remained at the forefront of theoretical and experimental research.¹ The main source of interest in these systems is the phenomenon of colossal magnetoresistance (CMR), which they exhibit and is likely to have important technological applications. In the meantime, the underlying basic physics remains elusive and probably involves the strongly correlated nature of the doped magnetic oxides. The CMR in doped manganates is observed for intermediate hole-doping levels, typically $0.2 \leq x \leq 0.5$, in the temperature region around the transition between low-temperature metallic ferromagnetic (FM) and high-temperature insulating paramagnetic phases. In addition to double-exchange ferromagnetism,² the CMR compounds also possess pronounced antiferromagnetic (AFM) tendencies, as evident from the AFM spin ordering with Néel temperatures of about 100–200 K, observed^{3,4} at the doping end points ($x=0$ and $x=1$). This antiferromagnetism is of a superexchange origin.⁵

The manganates' physics involves several degrees of freedom of substantially different natures, including localized core spins S_i of Mn ions, fermionic degrees of freedom associated with conduction e_g electrons, lattice distortions, *etc.* In such systems, the presence of competing interactions (such as FM and AFM) often gives rise to phase separation,^{6–9} whereby areas of different phases are stabilized in a structurally and stoichiometrically homogeneous sample. In the case of the manganates, it has even been suggested^{7,10} that phase separation into insulating paramagnetic and metallic FM phases may explain the resistivity peak observed near the Curie temperature. In the present paper, we focus on the low-temperature regime, where the presence of phase separation in the appropriate manganate systems has been directly verified, e.g., by means of scanning-tunneling microscopy (STM) on thin films.¹¹ Transport measurements reveal metastability and history dependence near the percolation threshold ($x \approx 0.2$), confirming phase separation in both film^{12,13} and crystalline^{14,15} samples.

Using simple microscopic models,^{2,16} it can readily be shown¹⁶ that the hole concentration x indeed controls the

balance between the FM and AFM tendencies of the system. Once x is tuned away from the optimal CMR doping region, the homogeneous FM metallic state no longer corresponds to the energy minimum. Instead, energy can be gained by changing the magnetic ordering, carrier density, band structure, and/or orbital state in *part* of the system, making the sample inhomogeneous.^{6–9,16,17} The surface tension between different phases^{16,18} then competes against the long range interactions present in the system in the form of electrostatic forces^{6,16,19,20} or long range crystal strain fields.^{21,22} These require that the system remain homogeneous at least *on average* on the appropriate length scale (such as the Debye-Hückel screening length), resulting in a periodic arrangement of nano- or mesoscopic regions of different phases.^{6,7} The geometry of the ensuing inhomogeneous (phase-separated) state is the focus of our present study.

Early studies of phase separation in double-exchange–superexchange systems^{6,16,23} implicitly assumed that the effects of the discrete lattice are unimportant, and consequently treated the problem within the continuum-based, long-wavelength approach. Within this framework, the optimal phase-separation geometry at small values of the FM volume (or area) fraction m (also the average magnetization per site) is obviously that of spherical (in two dimensions, circular) FM droplets located at the sites of a packed hexagonal (triangular) superlattice. To the best of our knowledge, only the three-dimensional case was treated in detail, with the implication that in two dimensions the situation is similar. When the system parameters are varied in such a way that m increases beyond $1/2$, the geometry changes to that of spherical AFM droplets in an otherwise FM matrix. The change generally occurs via a direct “geometrical phase transition”²³ without any intervening regime characterized by both phases forming infinite connected shapes (such as filaments and planar slabs in three dimensions or stripes in two dimensions).^{6,16,24}

This latter conclusion is important since such slab or stripe arrangements, if realized, would have been characterized by peculiar and potentially useful properties such as history-dependent anisotropy of the ground-state resistivity.

However, the continuum treatment, which is the basis of this result, is not valid beyond the region of very small values of $x \ll 1$. Indeed, recent studies suggest^{17,18} that the boundary between the two phases is abrupt on the lattice-spacing scale (i.e., of the type commonly associated with Ising spin systems). Such a boundary cannot be adequately described in the continuum limit, and its surface tension depends on its orientation with respect to the crystalline axes.¹⁸ This directional dependence of boundary energies should in turn affect the droplet shape (generally favoring diamond-shaped droplets in two dimensions),¹⁸ the arrangement of droplets in space, and ultimately the way the geometry of phase separation evolves with varying m . This is apparently a generic property of electronic phase separation, found also within the frameworks of Falikov-Kimball²⁵ and t - J (Ref. 26) models.

In the present paper, we revisit the problem within the framework of a single-orbital double-exchange–superexchange Hamiltonian (with infinite Hund’s coupling J_H), augmented by a long range Coulomb interaction term. Using a variational Hartree-Fock (HF) approach, we compute the energies of various two-dimensional droplet and stripe phases corresponding to a FM area fraction $m \lesssim 1/2$, and determine the optimal configuration. Our most important finding is that while a droplet lattice exists at low doping levels, a striped arrangement has a lower energy and is therefore stabilized over a broad region of the phase diagram. As anticipated from our previous results concerning the orientational dependence of the boundary energy,¹⁸ we find that diamond droplets and diagonal stripes are the preferred geometries for the FM regions of the inhomogeneous states. These conclusions gain further support from unrestricted Hartree-Fock calculations which we have carried out using Monte Carlo (MC)–simulated annealing on moderate-size clusters. The simulations also demonstrate the existence of inhomogeneous states comprised of AFM droplets (or stripes) embedded in a FM background ($m \gtrsim 1/2$), at higher doping levels. While our results pertain to the two-dimensional case, it is likely that qualitatively our conclusions would also apply to three-dimensional systems. Specifically, we suggest that a phase-separated state with filament or slab geometry (rather than a lattice of droplets) is realized for a certain range of parameters in three dimensions.

In addition, we find that the typical droplet size and stripe width do not exceed several lattice constants. This means that the motion of the charge carriers is strongly quantized, rendering droplets midway between metallic bulk and magnetic polarons²⁷ and giving rise to singularities in the stripe energy associated with the quantization of the transverse kinetic energy. This important property was not included in the earlier work,^{6,16,23} which assumed sufficiently large length scales for such quantum effects to be negligible. Our approach, on the other hand, allows one to explore the crossover between the regime of singly-occupied magnetic polarons, which appear for strong Coulomb and AFM couplings, and the more conventional phase-separation behavior where each metallic droplet is populated by many charge carriers.

The paper is organized as follows: in Sec. II, we introduce the model and briefly review the physics underlying phase

separation and magnetic-polaron formation in the absence of a long range force. A brief description of the calculational methods which were implemented in order to include the effects of the long range Coulomb repulsion appears in Sec. III, while the mass of details is relegated to Appendixes A and B. Section IV contains a detailed description of our Hartree-Fock and Monte Carlo results. We conclude with a brief discussion of the results in the context of current experimental and theoretical work (Sec. V). While an arrangement of conducting and insulating stripes in doped manganate films has not yet been observed, we suggest that present experimental knowledge should allow for a meaningful and successful research effort in this direction.

II. MODEL AND ITS PROPERTIES IN THE NONINTERACTING LIMIT

The starting point for the following calculation is the two-dimensional double-exchange Hamiltonian, generalized to include the superexchange coupling and the long range Coulomb interaction,

$$\begin{aligned} \mathcal{H} = & -\frac{t}{2} \sum_{\langle i,j \rangle \alpha} (c_{i\alpha}^\dagger c_{j\alpha} + \text{H.c.}) \\ & + \frac{J}{S^2} \sum_{\langle i,j \rangle} \mathbf{S}_i \cdot \mathbf{S}_j - \frac{J_H}{2S} \sum_{i,\alpha,\beta} \mathbf{S}_i \cdot (c_{i\alpha}^\dagger \boldsymbol{\sigma}_{\alpha\beta} c_{i\beta}) \\ & + U \sum_{i \neq j, \alpha, \beta} \frac{1}{|\mathbf{r}_i - \mathbf{r}_j|} (c_{i\alpha}^\dagger c_{i\alpha} - x)(c_{j\beta}^\dagger c_{j\beta} - x). \end{aligned} \quad (1)$$

Here t is the nearest-neighbor hopping amplitude and $c_{j\alpha}$ annihilates a conduction electron of spin $\alpha = \uparrow, \downarrow$ at site j of a square lattice. \mathbf{S}_i denotes the core spin made of three d -shell electrons ($S=3/2$) localized at site i , whose AFM superexchange interaction with neighboring core spins is given by the second term in \mathcal{H} . The third term arises from Hund’s coupling between the core spins and the conduction electrons, where the spin operator for the conduction electrons on site i involves the Pauli matrices $\boldsymbol{\sigma}$. It is this term, in conjunction with the fact that the hopping preserves the electronic spin, which gives rise to the double-exchange mechanism. This favors a FM spin configuration in order to reduce the conduction electrons’ kinetic energy.² The last term includes the Coulomb interaction among the conduction electrons, whose average density is x , and a neutralizing uniform positive background, created by the donors. Owing to the long range nature of the Coulomb interaction, the atomic-scale inhomogeneities of this background in real systems (created by chemical substitution) are not expected to be important from the point of view of our main purpose of comparing the energies of various inhomogeneous phases. This is because such energies always involve integration over volume.

In using the simplified model, Eq. (1), we neglect some additional physics characteristic of the CMR manganates.¹ This includes the presence of two (rather than one) conduction-electron e_g bands and the electron-lattice coupling. The logics behind this simplification are summarized, e.g., in Ref. 9: it is assumed that the mechanism for phase

separation (charge ordering) is the competition between ferro- and antiferromagnetism in the presence of a long range Coulomb repulsion [all contained in Eq. (1)]. Once the charge ordering is established, in a real system the orbital ordering (and the lattice distortions) would follow, leading to a quantitative renormalization of the parameter values. The model, Eq. (1), is however expected to suffice for a qualitative study of the generic features of the phase diagram while its simplicity allows one to maintain clarity of analysis. Further arguments regarding the expected model independence of our conclusions shall be given in Sec. V.

The relatively large value S of the Mn core spins means that their fluctuations are small, particularly in the $T \rightarrow 0$ limit considered here. In the following we assume $S \gg 1$ and treat the core spins classically. Consequently, the effective Hamiltonian governing the physics of the conduction electrons is determined by the configuration of the classical spins $\{S_i\}$. As far as Hund's coupling is concerned, the manganates are characterized by a moderate bare $J_H \lesssim t$. However, they also include a strong Hubbard on-site repulsion, $U_0 \gg t$, which significantly renormalizes J_H toward the strong-coupling limit.²⁸ Therefore, while we omit the Hubbard interaction from our Hamiltonian (1), we model its effects by taking $J_H \rightarrow \infty$.

Band-theory calculations^{9,29} suggest that typical values of the hopping amplitude t in the CMR manganates lie between 0.3 and 0.5 eV. The value of J can be roughly estimated from the experimentally observed Néel temperatures in the fully doped or undoped (with no conduction e_g electrons or with no holes) case,^{3,4} $T_N \sim 100\text{--}200$ K, corresponding to $J \sim 5\text{--}10$ meV. The long range Coulomb interaction strength U for thin films is evaluated as $U = e^2 / (a_0 \bar{\epsilon})$. Here, e is the electron charge and $a_0 \approx 3.9$ Å is the lattice spacing. The effective dielectric constant $\bar{\epsilon}$ is given by the average of dielectric constant ϵ_s of the substrate and that of the air, $\bar{\epsilon} = (\epsilon_s + 1)/2$. Among the substances which can be used as substrates for manganate films, lanthanum aluminate and neodymium gallate have^{30,31} $\epsilon_s \approx 23$ and $\epsilon_s \approx 20$, yielding $U \approx 0.31$ eV and $U \approx 0.35$ eV, respectively. Dielectric properties of the third possible substrate, strontium titanate, are strongly dependent on temperature, with^{30,32} ϵ_s changing from 24 000 (corresponding to $U \approx 0.31$ meV) at 4.2 K to $\epsilon_s \approx 277$ ($U \approx 0.027$ eV) at 300 K. This suggests the possibility of experimentally varying the value of U by using different substrates and/or changing the temperature.

Theoretical investigations of the double-exchange–superexchange competition have a history of more than 40 years. It is by now firmly established^{6,7,17} that this competition is resolved not via a second-order phase transition from the FM state to a uniform state with a helical or canted magnetic ordering, but rather via separation of the sample into regions characterized by different spin arrangements and conduction-electron band structures. We will be interested in the case of phase separation into FM and AFM regions with abrupt Ising-type boundaries^{17,18} between them. This means that the resulting configuration of S_i remains collinear, with all core spins either parallel or antiparallel to a selected direction. Thus, it is possible to denote a spin state simply as $S_i/S \equiv S_i = \pm 1$, and the Hamiltonian of the conduction electrons becomes a function of $\{S_i\}$. The large Hund's exchange

coupling then forces the conduction electrons' spins to polarize parallel to the core spins, resulting³³ in the following distribution of hopping amplitudes for a given spin configuration $\{S_i\}$:

$$t_{ij}(\{S_i\}) = \begin{cases} -t, & i, j \text{ nearest neighbors and } S_i = S_j \\ 0, & \text{otherwise.} \end{cases} \quad (2)$$

After these simplifications, the Hamiltonian takes the form

$$\begin{aligned} \mathcal{H}(\{S_i\}) = & \frac{1}{2} \sum_{\langle i,j \rangle} (t_{ij}(\{S_i\}) c_i^\dagger c_j + \text{H.c.}) + J \sum_{\langle i,j \rangle} S_i S_j \\ & + U \sum_{i \neq j} \frac{1}{|\mathbf{r}_i - \mathbf{r}_j|} (c_i^\dagger c_i - x)(c_j^\dagger c_j - x). \end{aligned} \quad (3)$$

The model, Eq. (3), on the (bipartite) square lattice is invariant under the particle-hole transformation $c_i^\dagger \rightarrow (-1)^p c_i$, and $x \rightarrow 1 - x$, where p takes the values 0 and 1 on the two sublattices. As a result we note that in the following, x acquire the more general meaning of a carrier density, i.e., either the electronic density or the hole density relative to the half-filled state. We will now briefly review the ground-state properties of Hamiltonian (3) at $U=0$.

When the carrier density x is finite, the ground state of the system at $J \rightarrow 0$ is uniform and FM. With increasing J beyond a certain critical value $J_c(x)$, this uniform FM state eventually becomes destabilized, and a nonuniform ground state is obtained instead. In this *phase-separated* state only part of the system is occupied by the FM phase. We will be interested in the case in which the other part is a simple Néel antiferromagnet with zero charge-carrier density. A variational study¹⁷ showed that in two dimensions such a phase-separated state may be realized only for $J < J^* \approx 0.036$. At higher values of J the magnetic ordering in either the electron-rich or the electron-poor regions of the sample differs from that of a ferromagnet or a Néel antiferromagnet.

Thermodynamic equilibrium between macroscopic FM and AFM regions means that the thermodynamic potentials in the two phases are equal,

$$\Omega_{\text{FM}} = \Omega_{\text{AFM}}, \quad (4)$$

where

$$\Omega_{\text{FM}} = \int_{-\infty}^{\mu} (\epsilon - \mu) g(\epsilon) d\epsilon + 2J \quad (5)$$

and

$$\Omega_{\text{AFM}} = -2J. \quad (6)$$

$g(\epsilon)$ is the density of conduction-electron states in the FM region. Since the latter is large, $g(\epsilon)$ can be taken to be the two-dimensional tight-binding density of states, and boundary corrections may be neglected. By solving Eqs. (4)–(6) for the Fermi energy μ , one readily obtains the carrier density in the FM region, x_{FM} , via

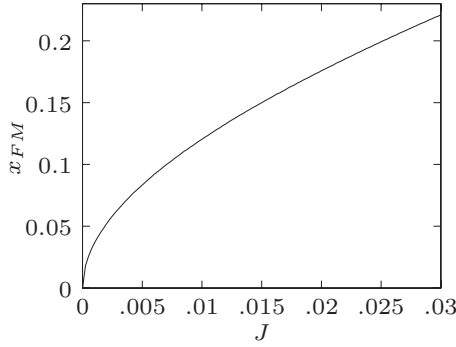


FIG. 1. The charge-carrier density x_{FM} in the FM region of a macroscopically phase-separated state.

$$x_{\text{FM}} = \int_{-\infty}^{\mu} g(\varepsilon) d\varepsilon, \quad (7)$$

with the result depicted in Fig. 1. The system remains in a uniform FM state as long as $x_{\text{FM}}(J) < x$. The fraction of the system area (or volume) occupied by the FM phase is given by $m = x/x_{\text{FM}}$. The critical value J_c for the onset of phase separation is then determined by the condition $x_{\text{FM}}(J_c) = x$.

In addition to the macroscopic phase separation as described above, the double-exchange–superexchange competition can also be resolved via an altogether different scenario (formation of magnetic polarons). When a single electron (or hole) is lodged into an antiferromagnetically ordered double-exchange magnet with zero charge carriers ($x = 0$), a free (self-trapped) magnetic polaron, or ferron,^{6,27,34–38} is formed around it. It is essentially a microscopic FM region, containing one charge carrier, in an otherwise AFM system. Since the propagation of charge is unimpeded in the FM region, it acts as a potential well for the sole carrier, which occupies the lowest bound state inside the

well. The polaron binding energy E_{mp} (with respect to the state where the AFM order is unperturbed) can be easily estimated.²⁷ We consider the case of a diamond-shaped polaron, with $L+1$ sites along each side (see Fig. 2, upper left). For $L \gg 1$ we find

$$E_{\text{mp}}(L) = -2t + \frac{t}{2} \left(\frac{\pi}{L+1} \right)^2 + 8L^2J, \quad (8)$$

where the first two terms are the ground-state energy of the charge carrier and the last one represents the superexchange contribution. Expression (8) should be minimized with respect to L , resulting in

$$E_{\text{mp}} = -2t + 4\pi\sqrt{Jt}. \quad (9)$$

Here, the coefficient of the second term depends on the geometry of the FM microregion (e.g., for a round polaron, one would have obtained 12.06 instead of 4π).

The above expressions are valid in the $J/t \ll 1$ regime [yielding $L \sim (t/J)^{1/4} \gg 1$], where it is easy to verify an important statement which is expected to hold for all J . Namely, if in the absence of a Coulomb interaction U , a second carrier is added to the system, it is energetically favorable for the two charge carriers to occupy the two lowest bound states in a *shared* FM microregion rather than to form two independent polarons. This conclusion is verified by calculating the binding energy of the (diamond-shaped) doubly-occupied polaron,

$$E_{\text{mp}}^{(2)} = -4t + 4\pi\sqrt{7Jt/2}, \quad (10)$$

which clearly satisfies $E_{\text{mp}}^{(2)} < 2E_{\text{mp}}$. This trend continues when further charge is added, and at $n \gg 1$ the binding energy (per carrier) of the n -carrier polaron decreases toward the limiting value E_{ps} ,

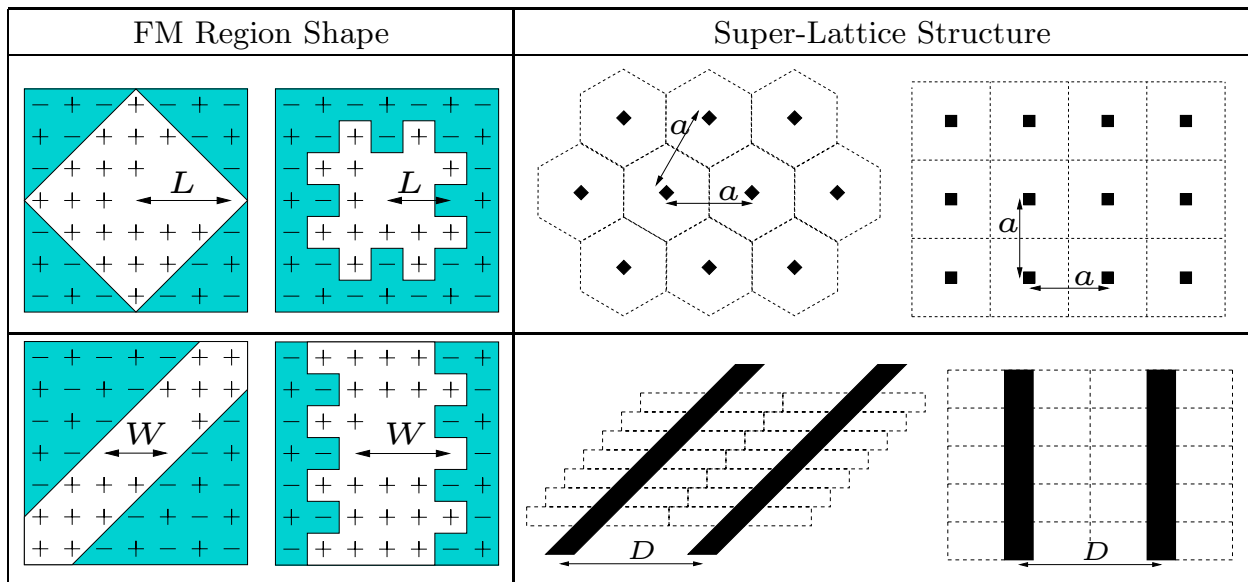


FIG. 2. (Color online) The geometry of the inhomogeneous configurations considered in the variational Hartree-Fock calculation. The dashed lines indicate the superlattice unit cell.

$$\frac{1}{n}E_{\text{mp}}^{(n)} \rightarrow E_{\text{ps}}, \quad (11)$$

which is the energy gain per carrier associated with the macroscopic phase-separated state. The latter can be evaluated as

$$E_{\text{ps}} = \frac{E_{\text{FM}} - E_{\text{AFM}}}{x_{\text{FM}}}, \quad (12)$$

where $E_{\text{FM}}(\mu) = \int_{-\infty}^{\mu} \varepsilon g(\varepsilon) d\varepsilon + 2J$ and $E_{\text{AFM}} = -2J$ are the energies per site of the FM and AFM phases. Using Eqs. (4) and (7) to evaluate μ and x_{FM} we find, in the limit $J \ll t$,

$$E_{\text{ps}} = -2t + 4\sqrt{\pi J t}. \quad (13)$$

The inequality $E_{\text{ps}} < E_{\text{mp}}$ implies that for any finite carrier density, at $U=0$, the double-exchange–superexchange competition is resolved via macroscopic phase separation.

Notwithstanding the preceding discussion, its conclusion may change if a realistically strong Coulomb interaction U is included, favoring a large spatial separation between the charge carriers. Indeed, as we demonstrate in the following, a polaronic state arises in the regime of large U and small carrier density. It is the extreme limit of a broad range of inhomogeneous states which originate from the frustration of macroscopic phase separation by long range forces. The study of this intermediate region of parameters lies at the focus of the remaining part of the paper. Since the typical size of the resulting FM regions is rather small, one needs to take into account the effects of quantization of the charge-carrier motion. At the same time, some of the results obtained for the macroscopic phase-separated system, such as the directional dependence of the boundary energy,¹⁸ still offer important guidance for the understanding of the inhomogeneous configurations. Next, we outline the methods used to treat this intermediate regime which is characterized by a combination of both traditional phase separation and magnetic-polaron (quantized) physics.

III. METHODS

A. Variational Hartree-Fock approach

Given Hamiltonian (3), our task is to find the configuration of core spins in the ground state. However, there is a vast multitude of possible spin configurations among which the ground state is to be sought, making it impossible to explore all of them. Nevertheless, previous studies of similar or related systems³⁹ suggest several families of highly symmetrical configurations as reasonable ground-state candidates. The two main types of spin configurations studied in this work are FM droplets in an AFM background and alternating FM and AFM stripes, as illustrated in Fig. 2. A uniform FM phase, in which the double-exchange mechanism completely overcomes the superexchange, is also considered.

Calculating the energy of the conduction electrons in a given configuration of core spins is a difficult problem. Here we suffice with the HF approximation, which gives an upper bound to their ground-state energy. Since we are dealing with periodic spin configurations, the HF equations for the whole system can be rewritten as an effective eigenvalue problem

within a single unit cell. The superexchange contribution to a configuration's energy is simply calculated by counting the number of FM and AFM bonds in a unit cell.

Based on previous analytical results¹⁸ and numerical investigations,³⁹ the considered droplets are either diamond or square shaped and are chosen to form either a triangular or square superlattice (see Fig. 2). Several droplet phases are possible by combining different droplet shapes and superlattice types. In addition, one has variational freedom to specify L , the size of the FM droplets, and n , the number of conduction electrons in each of the droplets. The distance between the droplets, a , is then uniquely determined by the type of superlattice, by n , and by the average density of conduction electrons, x .

The energy of each droplet phase is found by minimizing its energy density,

$$E_{\text{droplet}} = x \frac{E_{\text{HF,droplet}}}{n} + E_{J,\text{droplet}}, \quad (14)$$

with respect to the variational parameters, L and n . Here $E_{\text{HF,droplet}}$ is the HF energy of the conduction electrons inside a unit cell containing a single droplet, and $E_{J,\text{droplet}}$ is the AFM energy *per site*. The details of the HF calculation appear in Appendix A. The main source of complication is the necessity to take into account the Hartree interaction between electrons belonging to different droplets in the infinite superlattice. This is done by employing Ewald's summation method (see Appendix B). The AFM coupling energy per lattice site is

$$E_{J,\text{droplet}} = \begin{cases} -2J \left(1 - \frac{4L^2}{A} \right), & \text{diamond droplets} \\ -2J \left(1 - \frac{5L^2 - 8L + 8}{A} \right), & \text{square droplets,} \end{cases} \quad (15)$$

where $A = n/x$ is the area of a unit cell.

Two types of stripe phases were considered: diagonal and bond aligned. Additional variational freedom comes from the need to specify W , the stripe width, and x_{FM} , the (average) density of conduction electrons within the FM stripe. Just as for the droplet phase, the stripe phase energy is found by minimizing its energy density

$$E_{\text{stripe}} = x \frac{E_{\text{HF,stripe}}}{\lambda} + E_{J,\text{stripe}} \quad (16)$$

with respect to W and x_{FM} . Here λ and $E_{\text{HF,stripe}}$ are, respectively, the conduction electrons' number and energy per unit cell, and $E_{J,\text{stripe}}$ is the AFM energy per site. A unit cell in diagonal stripes is only one lattice spacing long in the direction along the stripe, and two spacings long in bond-aligned stripes (see Fig. 2); its width equals the stripe periodicity. Therefore,

$$\lambda = \begin{cases} x_{\text{FM}} W, & \text{diagonal stripes} \\ 2x_{\text{FM}} W & \text{bond-aligned stripes.} \end{cases} \quad (17)$$

λ , together with x , uniquely determine the distance between stripes D .

In a similar manner to the case of the droplet phase, when calculating the HF energy, one needs to take into account the Hartree interaction between the infinite number of unit cells in the systems. Moreover, the extended nature of the states along the stripes means that it is necessary to consider also the Fock exchange between different unit cells on the same stripe. A detailed account of the way this is done is presented in Appendix A. The AFM spin coupling energy per unit area for both diagonal and bond-aligned stripe phases is

$$E_{J,\text{stripe}} = -2J \left[1 - 2m \left(2 - \frac{1}{W} \right) \right], \quad (18)$$

where $m = x/x_{\text{FM}}$ is the fraction of FM regions in the system. By comparing the energies of all the above-mentioned phases, a phase diagram is constructed, depicting the nature of the ground state as a function of the external parameters, x , J/t and U/t .

B. Monte Carlo–simulated annealing

We have supplemented the calculation of the HF energy of various variational configurations by an *unrestricted* HF calculation using Monte Carlo–simulated annealing. In this method, the energy of a finite-size system is minimized with respect to the full configuration space of core spins, rather than a special subset of spin textures. In each Monte Carlo step the energy of a given configuration of classical core spins is evaluated using the HF approximation. A spin configuration is accepted as the system’s new state if the change in energy from the current state satisfies the Metropolis condition. The temperature is slowly decreased until the system reaches a stable low-energy configuration. If the temperature is decreased slowly enough, the final state is the HF approximation of the ground state.

The underlying assumption of the present study is that the system indeed separates into FM and AFM regions with an abrupt boundary between them. Therefore, the MC simulation needs to explore only such configurations, improving the convergence time. This can be achieved by setting all the spins on one sublattice to the “up” state, and incrementally flipping the spins on the other sublattice. An additional improvement comes from an algorithm used to decide which spin to flip. At first, a spin is chosen randomly. It is flipped if the resulting state satisfies the Metropolis criterion. If the spin is located near a FM-AFM boundary, then its neighbors are added to a queue of spins to be tested for flipping. After all the spins in the queue have been tested for a flip, a new spin is chosen randomly. Requiring that a spin be added to the queue no more than once prevents the simulation from repeating itself, thus maintaining ergodicity.

In our calculations, the system contained 24×24 sites arranged periodically on a torus. A linear annealing schedule was employed over 50–100 MC sweeps, and an identical number of sweeps at the lowest temperature allowed the system to thermalize into the ground state. The temperatures started from above $1.5J$ at the beginning of the annealing schedule to below $0.5J$ at its end.

Even though this method minimizes the system’s energy with respect to an unrestricted configuration space, it has a

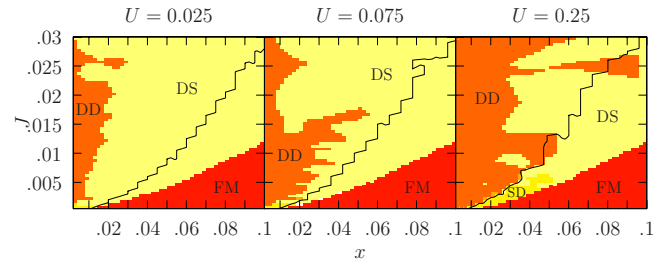


FIG. 3. (Color online) The HF phase diagram: DD—a triangular lattice of diamond-shaped droplets; SD—a square lattice of square droplets; DS—diagonal stripes; and FM—a uniform ferromagnet. The black lines correspond to $x/x_{\text{FM}} = 1/2$.

number of disadvantages when compared to the variational HF method, applied to only a number of special configurations. First, its periodicity is fixed; in our case it is 24 sites along each axis. In addition, the presence of long range interactions causes the simulations to converge very slowly. Nevertheless, it provides an important reference point with which the variational HF results may be contrasted, especially in order to confirm that the variational manifold contains the most relevant configurations.

IV. RESULTS

In the present section, we present and analyze our numerical results. The coupling constants J and U are measured in units of t , by setting the hopping amplitude $t = 1$. The HF energies of all the considered phases were calculated in the parameter range $x \leq 0.1$ and $J \leq 0.03$, and for three values of U , namely, $U = 0.025, 0.075, 0.25$. We chose to concentrate on this region on the x - J plane for two reasons. As already mentioned, a previous estimate¹⁷ sets $J^* = 0.036$ as the upper limit for the realization of a FM–Néel AFM (as opposed to other types of magnetic ordering) phase-separated state in two dimensions. Second, our calculations indicate that the line $x/x_{\text{FM}} = 1/2$ crosses $J = 0.03$ at $x^* = 0.1$; see Fig. 3. The region below this line on the x - J plane corresponds to configurations in which the FM phase occupies more than half the system area. While the stripes’ phases, which we consider, continue to be relevant in this region, we expect (and confirm in our MC simulations) that the phases of FM droplets ought to be replaced by configurations of AFM droplets embedded in a FM background. The latter turn out to be more involved computationally and were left out of the present study. We also wish to note that the above values of J^* and x^* are sensitive to the details of the considered model. Therefore, while experimentally percolation of the metallic phase at low temperatures is observed in manganates with $x \geq 0.18$, we expect our qualitative conclusions to apply to more complicated models of manganates as long as phase separation into FM and AFM phases is possible.

We begin our review of the results by discussing the phase diagram and presenting general arguments for its structure. We then move on to consider the details of the most dominant phases.

A. Phase diagram

The main result of our calculation is the phase diagram, Fig. 3, derived from the variational HF approach and depict-

ing the system's ground-state configuration as a function of the parameters x , J , and U . It demonstrates that diamond droplets in a triangular formation is the preferred phase at low densities, while diagonal stripes are prevalent at higher values of x . This stability of a striped phase is the most important result of our calculation. The striped arrangement is expected to possess unusual and potentially useful properties (see Sec. V, where we also mention possible directions of experimental search for the stripe phase in CMR manganates). When the Coulomb interaction strength U is increased, the transition between droplets and stripes occurs at higher x . As discussed above, our variational approach becomes insufficient below the line $x/x_{\text{FM}}=1/2$, as we do not allow for a phase of AFM droplets embedded in a FM background. Such a phase is expected to appear near the transition to the uniform FM state. This conclusion is supported by the unconstrained HF results presented below. We are unable, though, to map in detail the boundary between the stripe and droplet phases in this parameter regime.

The general features of the phase diagram can be explained by simple energy considerations. The preference of diagonal stripes and diamond droplets is a direct result of the lower energy of diagonal boundaries, as previously established by two of the authors.¹⁸ The appearance of a triangular droplet lattice at low densities is akin to the physics giving rise to the Wigner crystal in a dilute gas of electrons. Next, we elaborate on the reasons and nature of the transition between the droplet and stripe phases.

To this end, let us examine how the energy difference between the two phases evolves with x . As x increases, the distance between droplets or stripes diminishes, but our HF results indicate that the size of these FM regions and the electron density within them, x_{FM} , vary slowly in the vicinity of the phase transition. The combined difference between the kinetic and magnetic energies per electron of the two phases, $\Delta\varepsilon$, depends on x_{FM} and on the size and shape of the FM regions, but not on the distance between them. We therefore conclude that at the qualitative level, changes in $\Delta\varepsilon$ with x cannot be the driving force behind the transition. Instead, we concentrate on the doping dependence of the difference in the Coulomb energy per electron between droplets and stripes, $\Delta\phi$.

The Coulomb energy contains contributions coming from the interaction between charges within a single superlattice unit cell and between different cells. The neutrality of each unit cell (due to the positive background) implies that the dominant contribution to the Coulomb energy per electron originates from the intracell component. Simple dimensional analysis allows us to obtain an estimate for its behavior. The amount of positive background charge within a droplet unit cell is xa^2 , a being the interdroplet spacing. Thus, the Coulomb potential due to the positive background is $\phi_{\text{droplet}}^+ \approx -Uxa$. The interaction between electrons within a droplet generates $\phi_{\text{droplet}}^- \approx Ux_{\text{FM}}L$, where L is the droplet size. Since $m \equiv x/x_{\text{FM}} \approx L^2/a^2$, we have

$$\phi_{\text{droplet}} = \phi_{\text{droplet}}^- + \phi_{\text{droplet}}^+ \approx Ux_{\text{FM}}L(1 - \sqrt{m}). \quad (19)$$

The Coulomb energy in the stripe phase takes a different form. The amount of charge per unit length is $x_{\text{FM}}W = xD$,

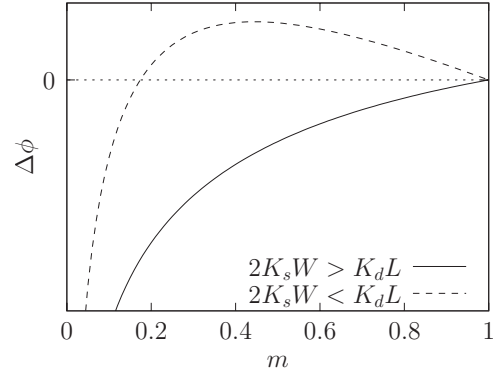


FIG. 4. Dimensional analysis form of $\Delta\phi$ as a function of m , demonstrating the difference between the two possible branches.

where W and D are the stripe width and the distance between stripes, correspondingly. The background potential is then $\phi_{\text{stripe}}^+ \approx Ux_{\text{FM}}W \ln D$ and the potential due to electrons in the same stripe is $\phi_{\text{stripe}}^- \approx -Ux_{\text{FM}}W \ln W$. Together they give

$$\phi_{\text{stripe}} = \phi_{\text{stripe}}^- + \phi_{\text{stripe}}^+ \approx -Ux_{\text{FM}}W \ln m, \quad (20)$$

where in this case $m=W/D$. Consequently, the difference in Coulomb energy per electron between the droplet and stripe phases has the form

$$\Delta\phi \equiv \phi_{\text{droplet}} - \phi_{\text{stripe}} \approx Ux_{\text{FM}}[K_dL(1 - \sqrt{m}) + K_sW \ln m], \quad (21)$$

where K_d and K_s are numerical constants characterizing the geometry of droplets and stripes, respectively. It is implicitly assumed in Eq. (21) that in the transition region between the phases x_{FM} is the same for both configurations (the HF calculation shows that this is correct up to 20%). The transition itself takes place at m^* , satisfying

$$\Delta\phi(m^*) + \Delta\varepsilon = 0, \quad (22)$$

where we have used the constancy of $\Delta\varepsilon$ near the transition.

If $2K_sW > K_dL$ then $\Delta\phi$ is a monotonously increasing function of m (in the physical range $0 < m < 1$); see Fig. 4. In this case at most a single solution m^* exists for condition (22), implying that the droplet phase is preferred when $m < m^*$, while stripes occur for $m > m^*$; the area of the droplet phase increases with U . On the other hand, if $2K_sW < K_dL$, $\Delta\phi$ acquires a maximum and two solutions, m_1^* and m_2^* , may appear. Under such conditions a re-entrant behavior follows; i.e., droplets are preferred when $m < m_1^*$ or $m > m_2^*$, and stripes are realized in the region $m_1^* < m < m_2^*$, which grows with increasing U . We note that in any case the existence of a solution to condition (22) crucially depends on the value of $\Delta\varepsilon$. It is the latter which reflects the features taken into account in the present work (viz., the orientational dependence of the boundary energy and the quantization of the carrier motion.)

Figure 5 shows HF results for $\Delta\phi$ and $(-\Delta\varepsilon)$ as functions of x for various values of J . Transitions between droplet and stripe phases occur when $\Delta\phi = -\Delta\varepsilon$. The division into discontinuous segments is due to changes in the properties of the stripes or droplets (the optimal values of W , L , and x_{FM} ;

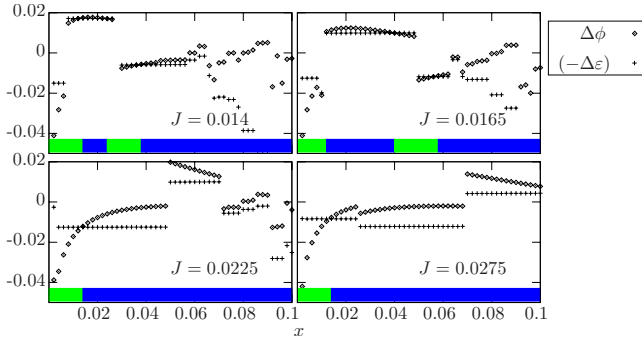


FIG. 5. (Color online) $\Delta\phi$ and $-\Delta\varepsilon$ as functions of x as obtained from the HF calculation for $U=0.075$ and various values of J . Below each plot are colored bands showing the ground-state configuration at the corresponding x values: green (light)—droplets; and blue (dark)—stripes. The transitions occur when $\Delta\phi = -\Delta\varepsilon$.

see below). However, the transitions generally do not occur at these points of discontinuity, leading to our previous assertions concerning the constancy of $\Delta\varepsilon$ and the dominant role of the Coulomb interaction in the vicinity of the transition. The first two transitions at $J=0.014$ and $J=0.0165$ are near a maximum in $\Delta\phi$, demonstrating the $2K_s W < K_d L$ branch behavior. Whereas these transitions occur on one continuous segment, the third transition occurs on a different segment, where only one solution exists. Other one-solution transitions are shown for $J=0.0225$ and $J=0.0275$.

B. Droplet phase

In general, a triangular lattice of diamond-shaped droplets proved to be energetically more favorable than the other types of droplet phases. As noted before this is a consequence of the directional dependence of the FM-AFM boundary energy and the minimization of the interdroplet Coulomb energy. Figure 6 shows the optimal droplet size L and the number of conduction electrons per droplet, n , as deduced from the variational HF calculation. Increasing the strength of the Coulomb repulsion has the obvious effect of decreasing the droplet size. Specifically, for the case of $U=0.25$ the variational study yields very small ($L=1,2$)

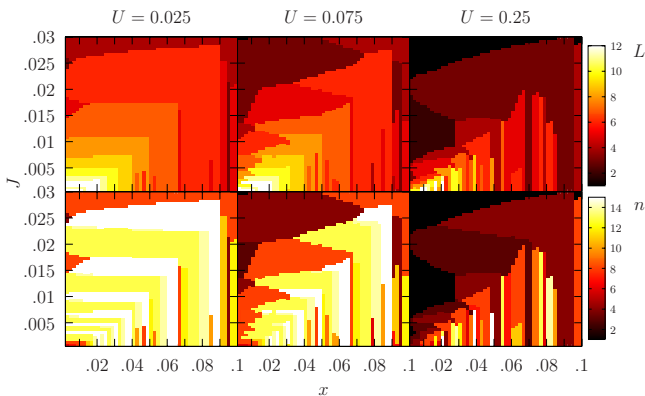


FIG. 6. (Color online) HF results for a triangular lattice of diamond droplets: optimal size L (top) and number of electrons per droplet n (bottom).

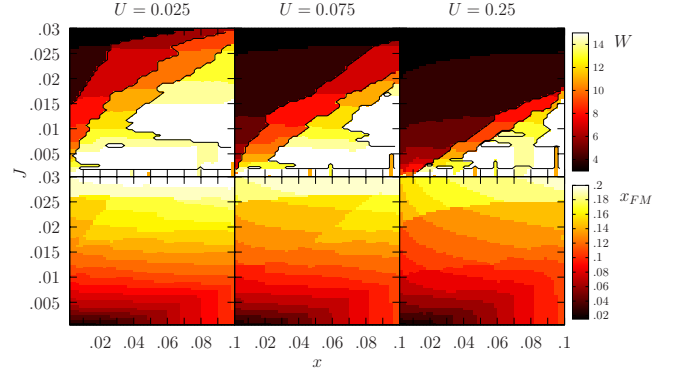


FIG. 7. (Color online) HF results for diagonal stripes: optimal W (top) and x_{FM} (bottom). The number of partially filled bands within a stripe changes across each black contour on the top panel.

singly-occupied droplets in the regime of low x and intermediate to large J . Comparing their energy to the other types of inhomogeneous states reveals that these *magnetic polarons* are in fact the lowest-energy configuration in this region of parameters; see the HF phase diagram, Fig. 3.

C. Stripe phase

Figure 7 shows the optimal stripe width W and conduction-electron density x_{FM} for diagonal stripes. The latter are more favorable than their bond-aligned counterparts due to the orientation dependence of the boundary energy. One striking feature in these HF results is the existence of abrupt transitions in the stripe width. A small increase in x may lead to a discontinuous change in W . On the other hand, increasing J typically leads to changes in W which are less steep. The electron density within the FM stripes, x_{FM} , varies, in general, very slowly with x and increases with J .

We use the condition of thermodynamic equilibrium, Eq. (4), between a diagonal FM stripe and its AFM environment to explain these features. The kinetic-energy contribution to the stripe's thermodynamic potential is determined by its noninteracting spectrum consisting of W bands (corresponding to the quantization of transverse electron motion within the stripe),

$$\varepsilon_b(k) = -t_b \cos\left(\frac{k}{2}\right), \quad (23)$$

where t_b is the bandwidth of band $b=1 \cdots W$,

$$t_b = 2t \cos\left(\frac{b\pi}{W+1}\right). \quad (24)$$

The resulting density of states in band b is then

$$g_b(\varepsilon) = \frac{2}{\pi t_b} \frac{1}{\sqrt{1 - (\varepsilon/t_b)^2}}, \quad (25)$$

which together with the chemical potential μ determines the number of electrons, n_b , per unit length in the band. Since we are interested in relatively low doping levels, we consider the lower $W/2$ bands for which

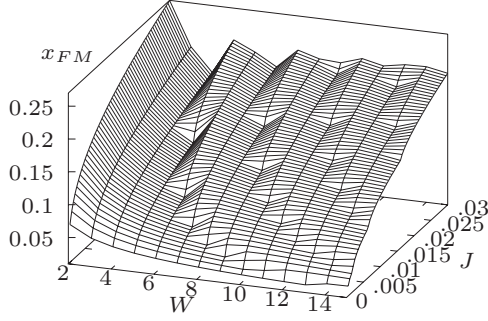


FIG. 8. x_{FM} in diagonal stripes of width W as imposed by thermodynamic equilibrium.

$$n_b = \int_{-t_b}^{\mu} g_b(\varepsilon) d\varepsilon = \frac{2}{\pi} \cos^{-1}\left(-\frac{\mu}{t_b}\right), \quad (26)$$

and the noninteracting electronic contribution to the total energy is

$$E_b = \int_{-t_b}^{\mu} \varepsilon g_b(\varepsilon) d\varepsilon = -\frac{2t_b}{\pi} \sin\left(\frac{\pi n_b}{2}\right). \quad (27)$$

Using these terms, the thermodynamic potential in the FM stripes is

$$\Omega_{\text{FM}}(W) = \frac{1}{W} \sum_b (E_b - \mu n_b) + 2J \left(1 - \frac{2}{W}\right), \quad (28)$$

where the second term is the magnetic energy, taking into account the structure of the boundaries. Ω_{AFM} remains the same as for an infinite AFM region [Eq. (6)]. Figure 8 shows $x_{\text{FM}} = \sum_b n_b / W$ evaluated at the Fermi energy μ which solves $\Omega_{\text{FM}}(W) = \Omega_{\text{AFM}}$ as a function of J and W .

Points of nonanalyticity occur whenever the chemical potential increases beyond the bottom of a band, $\mu = -t_b$, so that the carriers begin to fill this additional band. These nonanalyticities result in a corrugated landscape for $x_{\text{FM}}(W, J)$, shown in Fig. 8, whereby several values of W may correspond to the same x_{FM} . Thus, a small increase in x may drive an abrupt change in W but leave x_{FM} constant. This transition is accompanied by a change in the number of partially filled bands within the stripe, as depicted by the black contours in Fig. 7.

D. Simulation results

Although our Monte Carlo results are not sufficient for constructing the phase diagram, they yield convincing evidence that the phases included in the variational HF calculation are indeed the appropriate variational phases to consider. Some examples of ground states obtained by MC-simulated annealing are given in Fig. 9. Note that the moderate cluster size used in the simulation induces finite-size effects apparent, for example, in the imperfections of the stripe configurations. These results, in addition to results from other simu-

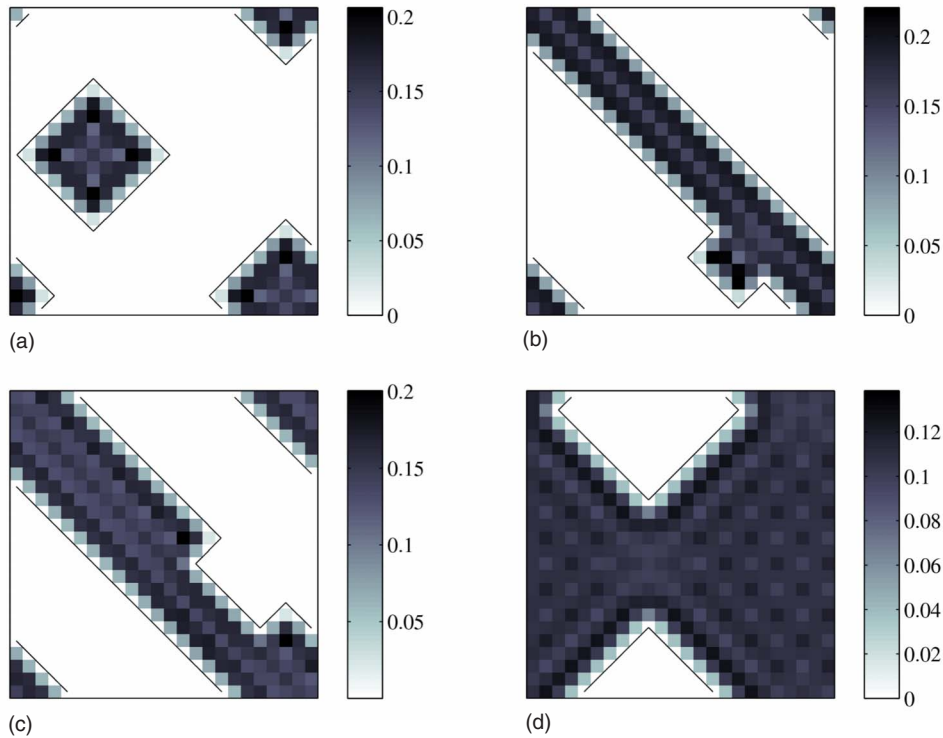


FIG. 9. (Color online) Electron density in ground states reached using simulated annealing. Top left: $x=0.0278$, $J=0.015$, and $U=0.075$. Top right: $x=0.0486$, $J=0.02$, and $U=0.05$. Bottom left: $x=0.0556$, $J=0.015$, and $U=0.05$. Bottom right: $x=0.0833$, $J=0.01$, and $U=0.05$. Dark lines outline FM-AFM boundaries.

lations done at other parameter values, agree with the general structure of the phase diagram in Fig. 3. Moreover, the unrestricted nature of the MC method yields also configurations with AFM droplets in a FM background (bottom right of Fig. 9). As mentioned before, such states were not considered in the variational HF approach because of the relative difficulty in calculating their HF energy. Nevertheless, there are reasons to believe, as confirmed by the simulations, that such a phase indeed exists around the transition line between the striped and uniform FM phases, where $m = x/x_{\text{FM}} > 1/2$.

V. DISCUSSION

The main finding of this paper concerns the geometry of the low-temperature phase-separated state in a two-dimensional double-exchange magnet. We did not invoke any lattice or orbital degrees of freedom but instead concentrated on the effects of the ubiquitous long range Coulomb interaction. We verified that when the relative area occupied by the FM phase, x/x_{FM} , is sufficiently large, a *striped arrangement* (rather than a droplet superlattice) is stabilized. Our results also confirm the expectation, based on a previous analysis of the directional dependence of the FM-AFM boundary energy,¹⁸ that diamond-shaped droplets and diagonal stripes are preferred over their square and bond-aligned counterparts. Indications to this effect are also present in other numerical studies of double-exchange models.³⁹

The stability of the stripe phase should not come as a surprise. In fact, even in the earlier studies, which considered the continuum limit,^{6,16} it was noted that the energies of the stripe and droplet configurations can be very close, although no parameter window was found where stripes would correspond to the lowest-energy configuration. As a result, it is conceivable, as indeed was shown in Ref. 40, that a stripe phase may be stabilized, even in this limit, once physics due to some sort of additional degrees of freedom is taken into account. Stripes also occur naturally in other models, such as t - J or Hubbard,⁴¹ which involve a competition between the AFM nature of a parent undoped state and the kinetic energy of the doped charge carriers. Long range AFM interaction was found to favor stripes in the FM Ising model.⁴² Regarding the case of a pure double-exchange system with Coulomb repulsion considered here, it has already been argued^{18,20} that the correct treatment of the boundaries between the FM and AFM regions is likely to tilt the balance in favor of a striped arrangement.

In the present work, we considered the experimentally relevant case of nanometer-size FM inclusions (comprising only a few lattice periods). Besides mapping the evolution of the geometry of the inhomogeneous system, we addressed the long-standing question regarding the stability of free magnetic polarons. As expected, we find polaronic behavior in the region of small carrier concentration $x \ll 1$ and strong Coulomb interaction. Away from this regime, individual magnetic polarons coalesce into larger FM areas. We were able to span the entire intermediate regime between the conventional phase separation (where the quantized character of the carrier motion becomes unimportant) and an array of free magnetic polarons (for which the notion of thermodynamic

equilibrium between FM and AFM phases becomes irrelevant). We emphasize that the two main physical ingredients underlying our findings, namely, the quantized electronic motion in small FM regions and the directional dependence of the boundary energy, can be viewed as largely model independent. Therefore, our present conclusions can be expected to stand for any double-exchange model with a long range interaction, including the case where the latter originates from crystal strain fields.^{21,22}

The bulk of our study was carried out using a variational HF approximation for the energy of various droplet and stripe phases. It was supplemented by unconstrained HF calculations on moderate-size clusters, implemented via Monte Carlo-simulated annealing. The HF approximation is expected to gain accuracy whenever the ratio of electrostatic energy to kinetic energy is small. Throughout the range of parameters studied by us, this ratio never exceeds 0.15. Moreover, since we deal with the case of fully polarized electronic spins, the spatial part of the many-body wave function is antisymmetric. This fact reduces correlation corrections to the HF result which stem from the tendency of any pair of electrons, owing to their mutual repulsion, to be more distant from each other than the HF wave function would indicate.

We close with a brief discussion of the experimental situation. To the best of our knowledge, a conclusive experimental observation of metallic stripes in phase-separated films of CMR materials is yet to be made. We note, however, that stripelike charge ordering on the atomic scale (charge-density wave) was observed in a variety of manganates. This includes films with different doping levels,⁴³ as well as ceramic⁴⁴ and single-crystal⁴⁵ samples in the insulating state above $x=0.5$. In addition, it was suggested⁴⁶ that the phase-separated state in a three-dimensional system may acquire a filament structure.

Nevertheless, we argue that it would be desirable to synthesize manganate films whose phase-separated state clearly exhibits metallic stripes. In addition to illustrating our theoretical picture, such systems are expected to display unique and potentially useful properties, some of which were not previously observed. One of these is an anisotropic conductance, whereby the stripes' direction determines a low-resistivity axis, which ought to be amenable to reorientation by, e.g., applying a voltage. In general, one expects to find history-dependent resistance and memory effects akin to and probably more pronounced than those observed earlier in phase-separated films,^{12,13} for which no evidence for stripes was reported. When the sample composition gets close to the one corresponding to a stable striped arrangement, weak perturbations such as external electric or magnetic fields may be sufficient to change the geometry of the FM regions from droplets to stripes, with a drastic change in transport properties in the form of colossal electroresistance due to dielectrophoresis⁴⁷ and large low-temperature magnetoresistance.

Which manganate system could potentially exhibit a metallic stripe order? In general, in order to look for such a state one is interested to explore the parameter space by changing the average carrier concentration x , the metallic area fraction m , and the strength U of the Coulomb interaction.⁴⁸ While x

is determined by the dopant concentration, the experimentally measurable quantity m depends, in our model, on the ratio of the AFM coupling J to the hopping t . The latter may be affected by, e.g., the choice of the rare-earth ion. An example of a system which apparently allows control over the value of m is $(\text{La}_{1-y}\text{Pr}_y)_{1-x}\text{Ca}_x\text{MnO}_3$. Three-dimensional crystals of this compound with x between 0.25 and 0.5 are metallic for $y=0$, with no signatures of phase separation at low temperatures.³ At $y=1$, the system is phase separated⁴⁹ and exhibits robust insulating behavior, presumably corresponding to well-separated metallic droplets in an insulating matrix. The properties of the phase-separated state change as one decreases the value of y , and at $y=0.7$ it is possible to observe conduction path formation and switching as a result of an applied current.¹⁵ Similar behavior is also found in thin films of the same compound, which at least for sufficiently large values of y are phase separated,⁵⁰ as reflected in their peculiar dielectric and transport properties.^{51,52}

These findings prompt us to suggest looking for signatures of stripes in $(\text{La}_{1-y}\text{Pr}_y)_{1-x}\text{Ca}_x\text{MnO}_3$ films by systematically varying y and with it, as indicated above, the relative area m of the metallic phase. We expect stripes to appear around the point where the areas of metallic and insulating phases are equal to each other. Besides $(\text{La}_{1-y}\text{Pr}_y)_{1-x}\text{Ca}_x\text{MnO}_3$, there are other hole-doped manganese systems which may exhibit a stripe geometry of phase separation; see Ref. 53. In addition, we expect our results to be relevant for some electron-doped manganates,⁵⁴ as well as possibly for Eu-based magnetic semiconductors.⁶

ACKNOWLEDGMENTS

The authors take pleasure in thanking R. Berkovits, J. T. Chalker, and G. Singh-Bhalla for enlightening discussions. This work was supported by the United States–Israel Binational Science Foundation (Grant No. 2004162). Support by the Israeli Absorption Ministry is also acknowledged.

APPENDIX A: HARTREE–FOCK EQUATIONS FOR A PERIODIC CONFIGURATION

The HF equations for n interacting spin-polarized electrons may be written in matrix form as an effective eigenvalue equation, which needs to be solved self-consistently,⁵⁵

$$\sum_{\mathbf{r}'} H_{\mathbf{r}\mathbf{r}'} \phi_{s\mathbf{r}'} = \varepsilon_s \phi_{s\mathbf{r}}, \quad (\text{A1})$$

where the effective Hamiltonian matrix is given by

$$H_{\mathbf{r}\mathbf{r}'} = h_{\mathbf{r}\mathbf{r}'} + \sum_{s=1}^n \left(\delta_{\mathbf{r}\mathbf{r}'} \sum_{\mathbf{r}''} v_{\mathbf{r}\mathbf{r}''} |\phi_{s\mathbf{r}''}|^2 - v_{\mathbf{r}\mathbf{r}'} \phi_{s\mathbf{r}'}^* \phi_{s\mathbf{r}} \right). \quad (\text{A2})$$

The indices \mathbf{r} , \mathbf{r}' , and \mathbf{r}'' indicate positions on the lattice, $h_{\mathbf{r}\mathbf{r}'}$ is the single-particle part of the Hamiltonian, and $v_{\mathbf{r}\mathbf{r}'}$ is the interaction energy of a particle at site \mathbf{r} and a particle at site \mathbf{r}' . $\phi_{s\mathbf{r}}$ are the eigenvectors in lattice-site representation, each indexed by label s and with ε_s as its eigenvalue. The self-

consistent solution yields the HF ground-state energy, given by

$$E = \frac{1}{2} \sum_{s=1}^n \left(\varepsilon_s + \sum_{\mathbf{r}\mathbf{r}'} \phi_{s\mathbf{r}}^* h_{\mathbf{r}\mathbf{r}'} \phi_{s\mathbf{r}'} \right), \quad (\text{A3})$$

where the summation is over the n states with lowest eigenvalues ε_s . For Hamiltonian (3) considered in the present study, the single-particle term is

$$h_{\mathbf{r}\mathbf{r}'} = \frac{t_{\mathbf{r}\mathbf{r}'}}{2} - \delta_{\mathbf{r}\mathbf{r}'} U x \int \frac{d\mathbf{R}}{|\mathbf{r} - \mathbf{R}|}, \quad (\text{A4})$$

with an implicit dependence, given by Eq. (2), of $t_{\mathbf{r}\mathbf{r}'}$ on the configuration of the core spins $\{\mathcal{S}_{\mathbf{r}}\}$. The second term in Eq. (A4) reflects the interaction between the conduction electrons and a *continuous* neutralizing positive background of density $x=n/A$, where A is the system area, via the Coulomb potential $v_{\mathbf{r}\mathbf{r}'} = U/|\mathbf{r} - \mathbf{r}'|$. Noting that the eigenvectors are normalized to unity, $\sum_{\mathbf{r}''} |\phi_{s\mathbf{r}''}|^2 = 1$, and that the $\mathbf{r} = \mathbf{r}''$ and $\mathbf{r} = \mathbf{r}'$ terms in Eq. (A2) are equal and opposite, we are led to analyze the following HF Hamiltonian:

$$H_{\mathbf{r}\mathbf{r}'} = \frac{t_{\mathbf{r}\mathbf{r}'}}{2} + U \sum_{s=1}^n \left[\delta_{\mathbf{r}\mathbf{r}'} \sum_{\mathbf{r}''} \left(\frac{1 - \delta_{\mathbf{r}\mathbf{r}''}}{|\mathbf{r} - \mathbf{r}''|} - \frac{1}{A} \int \frac{d\mathbf{R}}{|\mathbf{r} - \mathbf{R}|} \right) |\phi_{s\mathbf{r}''}|^2 - \frac{1 - \delta_{\mathbf{r}\mathbf{r}'}}{|\mathbf{r} - \mathbf{r}'|} \phi_{s\mathbf{r}'}^* \phi_{s\mathbf{r}} \right]. \quad (\text{A5})$$

We are interested in cases where the core spins' configuration is periodic, such that the system can be divided into N unit cells, each containing an identical configuration of spins on M sites. Let the superlattice vectors $\{\mathbf{l}\}$ identify the location of the unit cells. A position \mathbf{r} on the lattice can then be written as $\mathbf{r}(\mathbf{l}, i) = \mathbf{l} + \mathbf{r}_i$, where \mathbf{r}_i is the position within the unit cell \mathbf{l} , containing \mathbf{r} . The spin periodicity implies that $H_{\mathbf{r}\mathbf{r}'}$ between sites $\mathbf{r} = \mathbf{l} + \mathbf{r}_i$ and $\mathbf{r}' = \mathbf{l}' + \mathbf{r}_j$ depends only on i , j , and the superlattice vector $\mathbf{l}' = \mathbf{l} - \mathbf{l}$ connecting the two unit cells, i.e., $H_{\mathbf{r}\mathbf{r}'} = H_{ij}(\mathbf{l}'')$. As a consequence of Bloch's theorem, this means that the energy eigenfunctions, expressed in the (\mathbf{l}, i) representation, take the form $\phi_{bi}(\mathbf{k}) e^{i\mathbf{k}\cdot\mathbf{l}} / \sqrt{N}$, with eigenenergies $\varepsilon_b(\mathbf{k})$, where \mathbf{k} is defined within the first Brillouin zone of the reciprocal superlattice. The “band” index b runs from 1 to M , and $\phi_{bi}(\mathbf{k})$ is normalized to unity within a single unit cell. Written in the (\mathbf{k}, i) basis, the Hamiltonian becomes block diagonal, where the matrix elements of the block connecting states with the same \mathbf{k} are given by

$$H_{ij}(\mathbf{k}) = \frac{t_{ij}(\mathbf{k})}{2} + \frac{U}{N} \sum_{b, \mathbf{k}'} \Theta[\mu - \varepsilon_b(\mathbf{k}')] \left[\delta_{ij} \sum_{i'} v_{ii'}^H |\phi_{bi'}(\mathbf{k}')|^2 - v_{ij}(\mathbf{k} - \mathbf{k}') \phi_{bj'}^*(\mathbf{k}') \phi_{bi}(\mathbf{k}') \right]. \quad (\text{A6})$$

Here

$$t_{ij}(\mathbf{k}) = \sum_{\mathbf{l}} t_{ij}(\mathbf{l}) e^{-i\mathbf{k}\cdot\mathbf{l}} \quad (\text{A7})$$

is the Fourier transform of the hopping amplitudes $t_{ij}(\mathbf{l})$ between sites i and j in unit cells separated by a superlattice vector \mathbf{l} . We also introduced

$$v_{ij}(\mathbf{k}) = \sum_{\mathbf{l}} \frac{1 - \delta_{ij}\delta_{\mathbf{l},0}}{|\mathbf{l} + \mathbf{r}_i - \mathbf{r}_j|} e^{-i\mathbf{k}\cdot\mathbf{l}}, \quad (\text{A8})$$

$$v_{ii'}^H = v_{ii'}(0) - \frac{1}{A_{\text{uc}}} \int \frac{d\mathbf{R}}{|\mathbf{r}_i - \mathbf{R}|}, \quad (\text{A9})$$

where $A_{\text{uc}} = A/N$ is the area of a unit cell. The chemical potential μ is defined by $n = \sum_{b,\mathbf{k}} \Theta[\mu - \varepsilon_b(\mathbf{k})]$, with $\Theta(x)$ denoting the step function.

The HF ground-state energy of the conduction electrons is

$$E_{\text{el}} = \frac{1}{2} \sum_{b,\mathbf{k}} \left[\varepsilon_b(\mathbf{k}) + \frac{1}{2} \sum_{ij} \phi_{bi}^*(\mathbf{k}) t_{ij}(\mathbf{k}) \phi_{bj}(\mathbf{k}) \right] \Theta[\mu - \varepsilon_b(\mathbf{k})] - \frac{1}{2} U n x \int \frac{d\mathbf{R}}{|\mathbf{R}|}, \quad (\text{A10})$$

where in the last term we have taken the limit $N \rightarrow \infty$. This diverging contribution is canceled by the self-interaction of the positive background, evaluated in the same limit,

$$E_{\text{bg}} = \frac{1}{2} U x^2 \int \frac{d\mathbf{R} d\mathbf{R}'}{|\mathbf{R} - \mathbf{R}'|} = \frac{1}{2} U n x \int \frac{d\mathbf{R}}{|\mathbf{R}|}. \quad (\text{A11})$$

Consequently, the total energy (not including the contribution of the antiferromagnetic interaction between the core spins) is given by the sum over b and \mathbf{k} in Eq. (A10).

In order to evaluate the matrix elements of the HF Hamiltonian, we need a method for calculating the infinite superlattice sums in Eqs. (A7)–(A9). The first of these is trivial since hopping is allowed only between nearest-neighbor sites within a unit cell or between adjacent ones. In two dimensions this leaves at most five terms to the sum. On the other hand, the Coulomb interaction is long ranged, and an infinite number of terms need to be included in Eqs. (A8) and (A9).

1. Hartree term

Hartree interaction matrix (A9) includes two diverging contributions, one coming from the interaction with the average electronic density and the other from the interaction with the positive uniform background. The two contributions cancel each other. In order to demonstrate this and extract the remaining finite piece, we employ Ewald's summation (see Appendix B). The main identity of this method, directly applicable to the evaluation of the first term in Eq. (A9), is

$$\sum_{\mathbf{l}} \frac{1}{|\mathbf{l} + \mathbf{r}|} = \frac{2\pi}{A_{\text{uc}}} \sum_{\mathbf{g}} \frac{e^{i\mathbf{g}\cdot\mathbf{r}}}{|\mathbf{g}|} \text{erfc}\left(\frac{|\mathbf{g}|}{2G}\right) + \sum_{\mathbf{l}} \frac{1}{|\mathbf{l} + \mathbf{r}|} \text{erfc}(G|\mathbf{l} + \mathbf{r}|). \quad (\text{A12})$$

As before, \mathbf{l} are the superlattice vectors and A_{uc} is the unit-cell area. Here, \mathbf{g} are the reciprocal superlattice vectors, and

G is an arbitrary constant, chosen to minimize the number of relevant terms in both sums controlled by the complementary error function $\text{erfc}(x)$. Note that the divergence which stems from summing over large \mathbf{l} vectors in the left-hand side of Eq. (A12) is encoded in the $\mathbf{g}=0$ term on the right-hand side. This divergence is canceled by the integral over the whole system in Eq. (A9). This can be readily seen by using Eq. (A12) with $G \rightarrow \infty$, writing it as

$$\frac{1}{A_{\text{uc}}} \int \frac{d\mathbf{r}}{|\mathbf{r}|} = \frac{1}{A_{\text{uc}}} \int_{\text{uc}} d\mathbf{r} \sum_{\mathbf{l}} \frac{1}{|\mathbf{l} + \mathbf{r}|} = \frac{2\pi}{A_{\text{uc}}} \sum_{\mathbf{g}} \frac{\delta_{\mathbf{g},0}}{|\mathbf{g}|}. \quad (\text{A13})$$

Consequently we find for the Hartree matrix

$$v_{ii'}^H = \frac{2\pi}{A_{\text{uc}}} \sum_{\mathbf{g} \neq 0} \frac{e^{i\mathbf{g}\cdot\mathbf{r}_{ii'}}}{|\mathbf{g}|} \text{erfc}\left(\frac{|\mathbf{g}|}{2G}\right) - \frac{2\sqrt{\pi}}{A_{\text{uc}}G} + \sum_{\mathbf{l} \neq 0} \frac{1}{|\mathbf{l} + \mathbf{r}_{ii'}|} \text{erfc}(G|\mathbf{l} + \mathbf{r}_{ii'}|) + (1 - \delta_{ii'}) \frac{\text{erfc}(G|\mathbf{r}_{ii'}|)}{|\mathbf{r}_{ii'}|} - \delta_{ii'} \frac{2G}{\sqrt{\pi}}, \quad (\text{A14})$$

where $\mathbf{r}_{ii'} = \mathbf{r}_i - \mathbf{r}_{i'}$.

2. Droplets' Fock term

When the core spins are arranged in FM droplets separated by an AFM-ordered background, the conduction electrons cannot hop from one unit cell to the other, i.e., $t_{ij}(\mathbf{l}) = t_{ij}\delta_{\mathbf{l},0}$. Consequently $t_{ij}(\mathbf{k})$ is independent of \mathbf{k} ; see Eq. (A7). Under such a condition it is easy to verify that the HF eigenfunctions and eigenenergies are \mathbf{k} independent as well. To prove this assertion, let us assume that it is true and show that it leads to a \mathbf{k} -independent HF Hamiltonian, hence closing the argument self-consistently. Since the Hartree term in the HF Hamiltonian, Eq. (A6), depends on \mathbf{k} only through the HF eigenfunctions, it obviously fulfills the requirement. To complete the demonstration, we note that the same is true for the Fock term since it satisfies

$$H_{ij}^{\text{Fock}}(\mathbf{k}) = -\frac{U}{N} \sum_{b,\mathbf{k}'} \Theta(\mu - \varepsilon_b) v_{ij}(\mathbf{k} - \mathbf{k}') \phi_{bi}^* \phi_{bj} = -U \sum_b \Theta(\mu - \varepsilon_b) \frac{1 - \delta_{ij}}{|\mathbf{r}_i - \mathbf{r}_j|} \phi_{bi}^* \phi_{bj}. \quad (\text{A15})$$

Moreover, Eq. (A15) implies that in the case of FM droplets the calculation of the Fock term involves only a finite sum (over the M states within each droplet). This is a direct consequence of the vanishing overlap between electronic states in different droplets.

3. Stripes' Fock term

When the core spins are arranged in a striped configuration, hopping is allowed between unit cells along the direction of the stripes. In other words, if we decompose the superlattice vectors as $\mathbf{l} = n_a \mathbf{a} + n_b \mathbf{b}$, where \mathbf{a} and \mathbf{b} are primitive vectors along and off the stripe direction, respectively, then $t_{ij}(n_a, n_b) = t_{ij}(n_a) \delta_{n_b,0}$. As a result $t_{ij}(\mathbf{k})$ depends only on the \mathbf{k} component along the stripes, i.e., $t_{ij}(\mathbf{k}) = t_{ij}(k_a)$. It follows then, using the same reasoning presented above for the drop-

let case, that the HF eigenfunctions and eigenenergies depend only on k_a , and the Fock term takes the form

$$H_{ij}^{\text{Fock}}(k_a) = -\frac{U}{N_{a,b,k'_a}} \sum \Theta[\mu - \varepsilon_b(k'_a)] \phi_{bi}^*(k'_a) \phi_{bj}(k'_a) \times \sum_{n_a} \frac{1 - \delta_{ij} \delta_{n_a,0}}{|\mathbf{r}_{ij} + n_a \mathbf{a}|} e^{in_a(k_a - k'_a)a}, \quad (\text{A16})$$

where N_a is the number of unit cells along the stripe, $a=|\mathbf{a}|$, and \mathbf{r}_{ij} is the vector connecting sites i and j within a unit cell.

In contrast to the Hartree term where the interaction decays slowly, the exponential factor in the Fock exchange, Eq. (A16), ensures that the series converges relatively fast. Hence, the infinite sum is well approximated by assuming a long but finite stripe. In our calculation, we used $N_a = 100-200$ and verified that larger values change the ground-state energy by an insignificant amount. Note that the logarithmic divergence of the n_a sum in the case $k'_a = k_a$ is integrable and vanishes upon the summation over k'_a .

APPENDIX B: EWALD'S SUMMATION IN TWO DIMENSIONS

The development (based on Ref. 56) of Ewald's summation method begins by defining the function

$$F(\mathbf{r}, \rho) \equiv \frac{2}{\sqrt{\pi}} \sum_{\mathbf{l}} e^{-|\mathbf{l} + \mathbf{r}|^2 \rho^2}, \quad (\text{B1})$$

where the vectors $\{\mathbf{l}\}$ correspond to the N points of a two-dimensional lattice of area A . F is a periodic function of \mathbf{r} , with the periodicity of the lattice. Therefore, it can be expanded into the following Fourier series:

$$F(\mathbf{r}, \rho) = \sum_{\mathbf{g}} F_{\mathbf{g}}(\rho) e^{i\mathbf{g} \cdot \mathbf{r}}, \quad (\text{B2})$$

where $\{\mathbf{g}\}$ are the reciprocal lattice vectors, and

$$F_{\mathbf{g}}(\rho) = \frac{2}{\sqrt{\pi}} \frac{1}{A} \int d^2 r \sum_{\mathbf{l}} e^{-|\mathbf{l} + \mathbf{r}|^2 \rho^2} e^{-i\mathbf{g} \cdot \mathbf{r}} = \frac{2}{\sqrt{\pi}} \frac{N}{A} \int d^2 r e^{-|\mathbf{r}|^2 \rho^2 - i\mathbf{g} \cdot \mathbf{r}} = \frac{2\sqrt{\pi}}{A_{\text{uc}} \rho^2} e^{-|\mathbf{g}|^2 / 4\rho^2}. \quad (\text{B3})$$

Here, $A_{\text{uc}} = A/N$ is the area of a unit cell. Using Eqs. (B2) and (B3) and the identity

$$\frac{1}{|\mathbf{l} + \mathbf{r}|} = \frac{2}{\sqrt{\pi}} \int_0^\infty d\rho e^{-|\mathbf{l} + \mathbf{r}|^2 \rho^2}, \quad (\text{B4})$$

we obtain

$$\sum_{\mathbf{l}} \frac{1}{|\mathbf{l} + \mathbf{r}|} = \frac{2}{\sqrt{\pi}} \sum_{\mathbf{l}} \int_0^\infty d\rho e^{-|\mathbf{l} + \mathbf{r}|^2 \rho^2} = \frac{2\sqrt{\pi}}{A_{\text{uc}}} \sum_{\mathbf{g}} \int_0^G d\rho \frac{1}{\rho^2} e^{-|\mathbf{g}|^2 / 4\rho^2 + i\mathbf{g} \cdot \mathbf{r}} + \frac{2}{\sqrt{\pi}} \sum_{\mathbf{l}} \int_G^\infty d\rho e^{-|\mathbf{l} + \mathbf{r}|^2 \rho^2}, \quad (\text{B5})$$

where the integral was split into two at an arbitrary positive value G . Finally, calculating the integrals leads to Eq. (A12), where the divergent piece of the original sum is given by the $\mathbf{g}=0$ term (and when $\mathbf{r}=0$ also the $\mathbf{l}=0$ term) in the new representation. The remaining part of the infinite sums over \mathbf{g} and \mathbf{l} is rapidly converging at a rate which is optimized by an appropriate choice of G .

- ¹ *Colossal Magnetoresistive Oxides*, edited by Y. Tokura (Gordon and Breach, New York, 2000), and references therein.
- ² P.-G. de Gennes, *Phys. Rev.* **118**, 141 (1960).
- ³ P. Schiffer, A. P. Ramirez, W. Bao, and S.-W. Cheong, *Phys. Rev. Lett.* **75**, 3336 (1995).
- ⁴ C. Martin, A. Maignan, M. Hervieu, and B. Raveau, *Phys. Rev. B* **60**, 12191 (1999); J. F. Mitchell, C. D. Ling, J. E. Millburn, D. N. Argyriou, A. Berger, and M. Medarde, *J. Appl. Phys.* **89**, 6618 (2001).
- ⁵ Away from the doping end points, a partially filled spin-polarized conduction band gives rise to another AFM contribution, in addition to superexchange. See Ref. 28 for details.
- ⁶ E. L. Nagaev, *Colossal Magnetoresistance and Phase Separation in Magnetic Semiconductors* (Imperial College, London, 2002); *Phys. Rep.* **346**, 387 (2001), and references therein.
- ⁷ E. Dagotto, *Nanoscale Phase Separation and Colossal Magnetoresistance* (Springer, Berlin, 2003); E. Dagotto, T. Hotta, and A. Moreo, *Phys. Rep.* **344**, 1 (2001), and references therein.
- ⁸ D. P. Arovas, G. Gómez-Santos, and F. Guinea, *Phys. Rev. B* **59**, 13569 (1999); J. L. Alonso, L. A. Fernández, F. Guinea, V. Laliena, and V. Martín-Mayor, *ibid.* **63**, 064416 (2001); M. Yu. Kagan, K. I. Kugel, A. L. Rakhmanov, and D. I. Khomskii, *Fiz.*

- Nizk. Temp.* **27**, 815 (2001) [*Low Temp. Phys.* **27**, 601 (2001)]; N. D. Mathur and P. B. Littlewood, *Solid State Commun.* **119**, 271 (2001); D. Khomskii and L. Khomskii, *Phys. Rev. B* **67**, 052406 (2003); R. S. Fishman, F. Popescu, G. Alvarez, J. Moreno, T. Maier, and M. Jarrell, *New J. Phys.* **8**, 116 (2006).
- ⁹ S. K. Mishra, R. Pandit, and S. Satpathy, *J. Phys.: Condens. Matter* **11**, 8561 (1999).
- ¹⁰ M. Uehara, S. Mori, C. H. Chen, and S.-W. Cheong, *Nature (London)* **399**, 560 (1999).
- ¹¹ M. Fäth, S. Freisem, A. A. Menovsky, Y. Tomioka, J. Aarts, and J. A. Mydosh, *Science* **285**, 1540 (1999); A. Biswas, M. Rajeswari, R. C. Srivastava, T. Venkatesan, R. L. Greene, Q. Lu, A. L. de Lozanne, and A. J. Millis, *Phys. Rev. B* **63**, 184424 (2001).
- ¹² F. X. Hu and J. Gao, *Phys. Rev. B* **69**, 212413 (2004); J. Gao and F. X. Hu, *Appl. Phys. Lett.* **86**, 092504 (2005); A. Masuno, T. Terashima, Y. Shimakawa, and M. Takano, *ibid.* **85**, 6194 (2004); I. Pallecchi, L. Pellegrino, E. Bellingeri, A. S. Siri, and D. Marré, *Phys. Rev. B* **71**, 014406 (2005); A. Bhattacharya, M. Eblen-Zayas, N. E. Staley, A. L. Koblinskii, and A. M. Goldman, *ibid.* **72**, 132406 (2005); N. Takubo and K. Miyano, *ibid.* **76**, 184445 (2007).

- ¹³E. S. Vlahov, K. A. Nenkov, T. G. Donchev, E. S. Mateev, and R. A. Chakalov, *Vacuum* **76**, 249 (2004).
- ¹⁴A. Asamitsu, Y. Tomioka, H. Kuwahara, and Y. Tokura, *Nature (London)* **388**, 50 (1997); Y. Yuzhelevski, V. Markovich, V. Dikovskiy, E. Rozenberg, G. Gorodetsky, G. Jung, D. A. Shulyatev, and Ya. M. Mukovskii, *Phys. Rev. B* **64**, 224428 (2001); V. Markovich, G. Jung, Y. Yuzhelevski, G. Gorodetsky, A. Szewczyk, M. Gutowska, D. A. Shulyatev, and Ya. M. Mukovskii, *ibid.* **70**, 064414 (2004); V. Markovich, G. Jung, Y. Yuzhelevskiy, G. Gorodetsky, and Ya. M. Mukovskii, *Eur. Phys. J. B* **48**, 41 (2005); G. Garbarino, M. Monteverde, C. Acha, P. Levy, M. Quintero, T. Y. Koo, and S. W. Cheong, *Physica B* **354**, 16 (2004); L. Ghivelder and F. Parisi, *Phys. Rev. B* **71**, 184425 (2005); H. Jain, A. K. Raychaudhuri, Y. M. Mukovskii, and D. Shulyatev, *Appl. Phys. Lett.* **89**, 152116 (2006); H. Sakai and Y. Tokura, *ibid.* **92**, 102514 (2008).
- ¹⁵M. Tokunaga, Y. Tokunaga, and T. Tamegai, *Phys. Rev. Lett.* **93**, 037203 (2004).
- ¹⁶E. L. Nagaev, *Zh. Eksp. Teor. Fiz. Pis'ma Red.* **16**, 558 (1972) [*JETP Lett.* **16**, 394 (1972)]; V. A. Kashin and E. L. Nagaev, *Zh. Eksp. Teor. Fiz.* **66**, 2105 (1974) [*Sov. Phys. JETP* **39**, 1036 (1974)].
- ¹⁷D. I. Golosov, *J. Appl. Phys.* **91**, 7508 (2002).
- ¹⁸D. I. Golosov and D. Orgad, *Phys. Rev. B* **74**, 104403 (2006).
- ¹⁹L. Chayes, V. J. Emery, S. A. Kivelson, Z. Nussinov, and G. Tarjus, *Physica A* **225**, 129 (1996); Z. Nussinov, J. Rudnick, S. A. Kivelson, and L. N. Chayes, *Phys. Rev. Lett.* **83**, 472 (1999).
- ²⁰D. I. Golosov, *Phys. Rev. B* **67**, 064404 (2003).
- ²¹K. H. Ahn, T. Lookman, and A. R. Bishop, *Nature (London)* **428**, 401 (2004).
- ²²D. I. Khomskii and K. I. Kugel, *Europhys. Lett.* **55**, 208 (2001).
- ²³E. L. Nagaev, *Phys. Rev. B* **62**, 5751 (2000).
- ²⁴It was argued (Ref. 40), however, that the combined effects of a long range Coulomb interaction, polarizability, and the interaction of electrons with acoustical phonons may stabilize a slab structure in three dimensions.
- ²⁵N. Datta, A. Messenger, and B. Nachtergaele, *J. Stat. Phys.* **99**, 461 (2000); R. Lemański, J. K. Freericks, and G. Banach, *Phys. Rev. Lett.* **89**, 196403 (2002).
- ²⁶E. Eisenberg, R. Berkovits, D. A. Huse, and B. L. Altshuler, *Phys. Rev. B* **65**, 134437 (2002).
- ²⁷E. L. Nagaev, *Zh. Eksp. Teor. Fiz. Pis'ma Red.* **6**, 484 (1967) [*JETP Lett.* **6**, 18 (1967)]; *Zh. Eksp. Teor. Fiz.* **54**, 228 (1968) [*Sov. Phys. JETP* **27**, 122 (1968)]; *J. Magn. Magn. Mater.* **110**, 39 (1992), and references therein.
- ²⁸D. I. Golosov, *Phys. Rev. B* **71**, 014428 (2005).
- ²⁹S. Satpathy, Z. S. Popović, and F. R. Vukajlović, *Phys. Rev. Lett.* **76**, 960 (1996); J. E. Medvedeva, V. I. Anisimov, O. N. Mryasov, and A. J. Freeman, *J. Phys.: Condens. Matter* **14**, 4533 (2002).
- ³⁰E. A. Giess, R. L. Sandstrom, W. J. Gallagher, A. Gupta, S. L. Shinde, R. F. Cook, E. I. Cooper, E. J. M. O'Sullivan, J. M. Roldan, A. P. Segmüller, and J. Angilello, *IBM J. Res. Dev.* **34**, 916 (1990); J. Krupka, R. G. Geyer, M. Kuhn, and J. H. Hinken, *IEEE Trans. Microwave Theory Tech.* **42**, 1886 (1994).
- ³¹T. Konaka, M. Sato, H. Asano, and S. Kubo, *J. Supercond.* **4**, 283 (1991); J. Konopka and I. Wolff, *IEEE Trans. Microwave Theory Tech.* **40**, 2418 (1992).
- ³²E. Sawaguchi, A. Kikuchi, and Y. Kodera, *J. Phys. Soc. Jpn.* **17**, 1666 (1962); T. Sakudo and H. Unoki, *Phys. Rev. Lett.* **26**, 851 (1971).
- ³³P. W. Anderson and H. Hasegawa, *Phys. Rev.* **100**, 675 (1955).
- ³⁴W. Nolting, S. M. Jaya, and S. Rex, *Phys. Rev. B* **54**, 14455 (1996); M. J. Calderon, L. Brey, and P. B. Littlewood, *ibid.* **62**, 3368 (2000).
- ³⁵S. Pathak and S. Satpathy, *Phys. Rev. B* **63**, 214413 (2001); S. Thulasi and S. Satpathy, *Int. J. Mod. Phys. B* **18**, 3213 (2004).
- ³⁶V. M. Pereira, J. M. B. Lopes dos Santos, and A. H. Castro Neto, arXiv:0804.3094 (unpublished).
- ³⁷H. Meskine, T. Saha-Dasgupta, and S. Satpathy, *Phys. Rev. Lett.* **92**, 056401 (2004); H. Meskine and S. Satpathy, *J. Phys.: Condens. Matter* **17**, 1889 (2005).
- ³⁸M. Umehara, *Phys. Rev. B* **54**, 5523 (1996).
- ³⁹S. Kumar and P. Majumdar, *Phys. Rev. Lett.* **91**, 246602 (2003); **92**, 126602 (2004); S. Dong, H. Zhu, X. Wu, and J.-M. Liu, *Appl. Phys. Lett.* **86**, 022501 (2005); V. B. Shenoy, T. Gupta, H. R. Krishnamurthy, and T. V. Ramakrishnan, *Phys. Rev. Lett.* **98**, 097201 (2007).
- ⁴⁰E. L. Nagaev, *Phys. Rev. B* **64**, 014401 (2001).
- ⁴¹See, e.g., S. R. White and D. J. Scalapino, *Phys. Rev. Lett.* **80**, 1272 (1998); **81**, 3227 (1998); G. Hager, G. Wellein, E. Jeckelmann, and H. Fehske, *Phys. Rev. B* **71**, 075108 (2005); R. Citro and M. Marinaro, *Eur. Phys. J. B* **20**, 343 (2000); **22**, 343 (2001); M. Yu and H. Q. Lin, *Int. J. Mod. Phys. B* **19**, 299 (2005).
- ⁴²U. Löw, V. J. Emery, K. Fabricius, and S. A. Kivelson, *Phys. Rev. Lett.* **72**, 1918 (1994).
- ⁴³S. Mori, C. H. Chen, and S.-W. Cheong, *Nature (London)* **392**, 473 (1998); S. Cox, J. Singleton, R. D. McDonald, A. Migliori, and P. B. Littlewood, *Nature Mater.* **7**, 25 (2008); L. Sudheendra, V. Moshnyaga, E. D. Mishina, B. Damaschke, T. Rasing, and K. Samwer, *Phys. Rev. B* **75**, 172407 (2007).
- ⁴⁴J. C. Loudon, S. Cox, A. J. Williams, J. P. Attfield, P. B. Littlewood, P. A. Midgley, and N. D. Mathur, *Phys. Rev. Lett.* **94**, 097202 (2005), and references therein.
- ⁴⁵Ch. Renner, G. Aeppli, and H. M. Ronnow, *Mater. Sci. Eng., C* **25**, 775 (2005).
- ⁴⁶J. Tao, D. Niebieskikwiat, M. B. Salamon, and J. M. Zuo, *Phys. Rev. Lett.* **94**, 147206 (2005).
- ⁴⁷S. Dong, H. Zhu, and J.-M. Liu, *Phys. Rev. B* **76**, 132409 (2007).
- ⁴⁸Regarding the value of U , see discussion in Sec. II.
- ⁴⁹See, e.g., I. G. Deac, J. F. Mitchell, and P. Schiffer, *Phys. Rev. B* **63**, 172408 (2001); D. N. Argyriou, U. Ruett, C. P. Adams, J. W. Lynn, and J. F. Mitchell, *New J. Phys.* **6**, 195 (2004), and references therein.
- ⁵⁰T. Dhakal, J. Tosado, and A. Biswas, *Phys. Rev. B* **75**, 092404 (2007).
- ⁵¹H.-Y. Zhai, J. X. Ma, D. T. Gillaspie, X. G. Zhang, T. Z. Ward, E. W. Plummer, and J. Shen, *Phys. Rev. Lett.* **97**, 167201 (2006).
- ⁵²R. P. Rairigh, G. Singh-Bhalla, S. Tongay, T. Dhakal, A. Biswas, and A. F. Hebard, *Nat. Phys.* **3**, 551 (2007); G. Singh-Bhalla, S. Selcuk, T. Dhakal, A. Biswas, and A. Hebard, arXiv:0707.4411 (unpublished).
- ⁵³One of the candidates is $\text{Pr}_{1-x}(\text{Ca}_y\text{Sr}_{1-y})_x\text{MnO}_3$. In crystalline form, the y dependence of its properties was studied extensively [Y. Tomioka and Y. Tokura, *Phys. Rev. B* **66**, 104416 (2002)] Results obtained on patterned films at $y=0.35$ [T. Wu and J. F. Mitchell, *ibid.* **74**, 214423 (2006)] suggest current-driven formation of conducting stripes.

⁵⁴These include both lightly doped compounds such as $\text{Ca}_{1-x}\text{Sm}_x\text{MnO}_3$ with $x \sim 0.15$ [M. Respaud, J. M. Broto, H. Rakoto, J. Vanacken, P. Wagner, C. Martin, A. Maignan, and B. Raveau, *Phys. Rev. B* **63**, 144426 (2001)], and LaMnO_3 -doped with tetravalent ions [e.g., $\text{La}_{1-x}\text{Te}_x\text{MnO}_3$ or $\text{La}_{1-x}\text{Ce}_x\text{MnO}_3$, with $1+x e_g$ electrons per Mn site; see P. Raychaudhuri, C. Mitra, P. D. A. Mann, and S. Wirth, *J. Appl. Phys.* **93**, 8328

(2003); G. Tan, P. Duan, G. Yang, S. Dai, B. Cheng, Y. Zhou, H. Lu, and Z. Chen, *J. Phys.: Condens. Matter* **16**, 1447 (2004).

⁵⁵See, e.g., E. Merzbacher, *Quantum Mechanics* (Wiley, New York, 1970), Chap. 21.

⁵⁶See, e.g., J. M. Ziman, *Principles of the Theory of Solids* (Cambridge University Press, Cambridge, 1972).